Icarus 197 (2008) 137–151

Contents lists available at ScienceDirect

Icarus

www.elsevier.com/locate/icarus

The long-term stability of a possible aqueous ammonium sulfate ocean inside Titan

P.M. Grindrod [a,*], A.D. Fortes [a], F. Nimmo [b], D.L. Feltham [c], J.P. Brodholt [a], L. Vočadlo [a]

[a] Centre for Planetary Sciences, Department of Earth Sciences, University College London, Gower Street, London, WC1E 6BT, UK
[b] Department of Earth and Planetary Sciences, University of California at Santa Cruz, 1156 High Street, Santa Cruz, CA 95064-1077, USA
[c] Centre for Polar Observation and Modelling, Department of Earth Sciences, University College London, Gower Street, London, WC1E 6BT, UK

ARTICLE INFO

Article history:
Received 1 October 2007
Revised 3 April 2008
Available online 9 May 2008

Keywords:
Titan
Ices
Interiors
Thermal histories
Astrobiology

ABSTRACT

We model the thermal evolution of a subsurface ocean of aqueous ammonium sulfate inside Titan using a parameterized convection scheme. The cooling and crystallization of such an ocean depends on its heat flux balance, and is governed by the pressure-dependent melting temperatures at the top and bottom of the ocean. Using recent observations and previous experimental data, we present a nominal model which predicts the thickness of the ocean throughout the evolution of Titan; after 4.5 Ga we expect an aqueous ammonium sulfate ocean 56 km thick, overlain by a thick (176 km) heterogeneous crust of methane clathrate, ice I and ammonium sulfate. Underplating of the crust by ice I will give rise to compositional diapirs that are capable of rising through the crust and providing a mechanism for cryovolcanism at the surface. We have conducted a parameter space survey to account for possible variations in the nominal model, and find that for a wide range of plausible conditions, an ocean of aqueous ammonium sulfate can survive to the present day, which is consistent with the recent observations of Titan's spin state from Cassini radar data [Lorenz, R.D., Stiles, B.W., Kirk, R.L., Allison, M.D., del Marmo, P.P., Iess, L., Lunine, J.I., Ostro, S.J., Hensley, S., 2008. Science 319, 1649–1651].

1. Introduction

The general internal structure of Titan consists of a rocky core, overlain by an ice-rich mantle; depending on the exact P–T conditions at formation and at present, in addition to the chemical evolution surrounding the saturnian subnebula, this structure can include a subsurface ocean and an ice-rich crust (e.g., Tobie et al., 2006). Previous studies of a possible subsurface ocean inside Titan have concentrated on liquid compositions of water plus ammonia (e.g., Lunine and Stevenson, 1987; Grasset and Sotin, 1996; Fortes, 2000; Grasset et al., 2000; Sohl et al., 2003; Sotin and Tobie, 2004; Grasset and Pargamin, 2005; Tobie et al., 2006, 2005). The addition of ammonia lowers the freezing temperature of the liquid layer thus impeding complete crystallization of the ocean layer throughout Titan's evolution (e.g., Grasset and Sotin, 1996; Sotin et al., 1998; Grasset et al., 2000). However, as noted by Grasset et al. (2000), the composition of any possible subsurface ocean on Titan is likely to be complex, and may contain, in addition to ammonia, methane, nitrogen, and also hydrated salts, such as those expected at the icy Galilean satellites (e.g., Zimmer et al., 2000; Kivelson et al., 2002). In a recent study, Fortes et al. (2007) predicted a different internal structure for Titan, where a rocky core consisting of the hydrated mineral antigorite and a thin covering of brucite, is overlain by high pressure ice VI, an ocean consisting of aqueous ammonium sulfate and a crust made of methane clathrate with small amounts of ice I and ammonium sulfate. The freezing temperature of an ocean made of aqueous ammonium sulfate is about 250 K, significantly warmer than for a mixture of ammonia and water, and is therefore more prone to complete crystallization. Although such temperatures are expected inside the icy Galilean satellites (e.g., Zimmer et al., 2000; Kivelson et al., 2002), no previous study has addressed the possibility of a warm sulfate-rich ocean on Titan. Therefore, the problem we wish to address here is: can a subsurface ocean of aqueous ammonium sulfate survive inside Titan to the present day? We investigate this problem by using a parameterized convection model which is described in Section 2. We perform a parameter space study to determine under what conditions such an ocean can survive (Section 3) and then discuss the likelihood and implications of this ocean composition (Section 4).

2. Modeling

In order to investigate the temporal stability of an aqueous ammonium sulfate ocean, we model the thermal evolution of Titan using a parameterized convection method. Such studies of ther-

* Corresponding author. Fax: +44 (0) 20 7679 7833.
E-mail address: p.grindrod@ucl.ac.uk (P.M. Grindrod).

0019-1035/$ – see front matter
doi:10.1016/j.icarus.2008.04.006

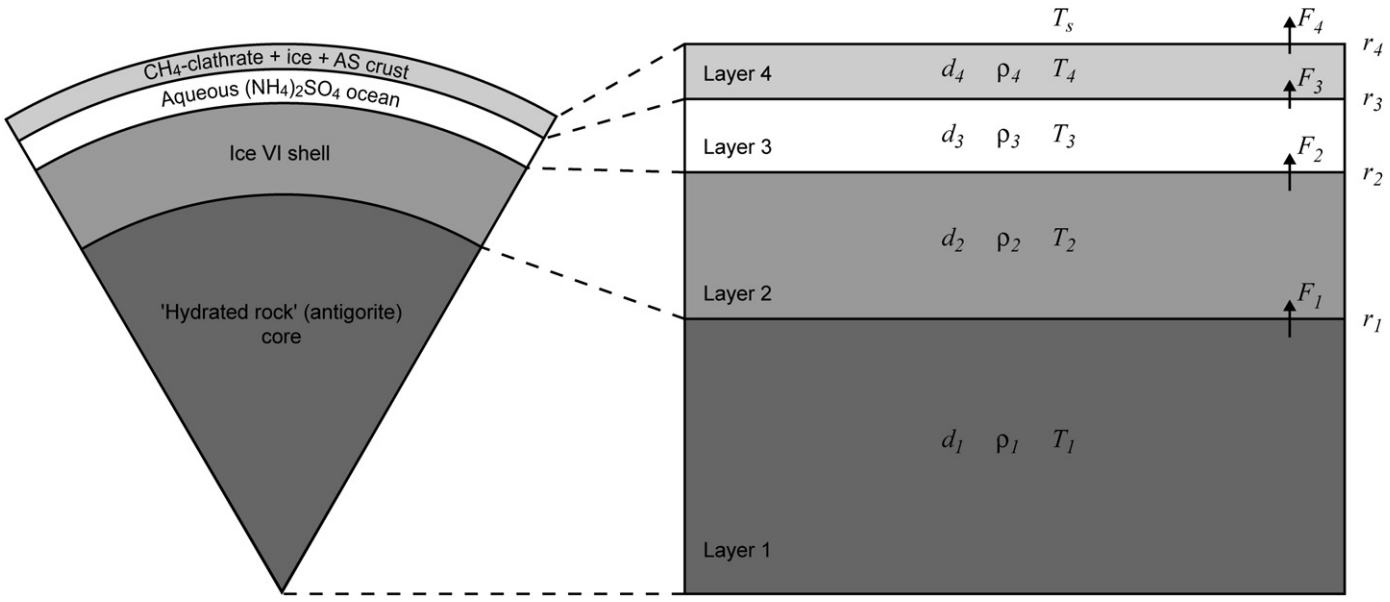

Fig. 1. Internal structure model of Titan used in this study. The figure on the left shows the material layers scaled to the starting thicknesses as described in Fortes et al. (2007). The figure on the right shows the notation scheme adopted for this study: layer 1 is the hydrated rock core, layer 2 the ice VI shell, layer 3 the aqueous ammonium sulfate ocean, and layer 4 the crust. Symbols used are defined in the text and typical values given in Table 1.

mal evolution have a rich history, including application to terrestrial planets (e.g., Phillips and Malin, 1983; Stevenson et al., 1983; Schubert et al., 1988; Solomatov, 1993; Nimmo and McKenzie, 1997; McNamara and van Keken, 2000; Nimmo and Stevenson, 2000; Hauck and Phillips, 2002; Nimmo et al., 2004) and icy bodies (e.g., Ellsworth and Schubert, 1983; Grasset and Sotin, 1996; Showman et al., 1997; Grasset et al., 2000; Sohl et al., 2003; Freeman, 2006). Although superseded by more detailed two- and three-dimensional convection models, parameterized schemes offer an efficient method of investigating a wide parameter space.

We use the new internal structure described above (Fortes et al., 2007) as the basis for a one-dimensional convection model (Fig. 1). Typical parameter values are given in Table 1. Due to its thinness, the hydroxide layer acts only as an extra conductive layer which we incorporate into the core, yielding a four layer model. We assume that convection is occurring in each layer (the validity of which is discussed later) and can be parameterized by relating the vigor of convection, the Rayleigh number (Ra), to the efficiency of convective heat transport, the Nusselt number (Nu). We then solve the equations for the conservation of energy as a function of time to determine the long-term stability of the ammonium sulfate ocean, and the overall thermal evolution of Titan. We advance three primary changes from previous studies of liquid shells inside Titan: (1) the effect of different Ra–Nu scaling laws, (2) an ocean of aqueous ammonium sulfate composition, and (3) a crust made of varying amounts of methane clathrate and ice Ih.

2.1. Parameterized convection and scaling laws

We use a standard parameterized convection method of solving an energy conservation equation for each layer. The thermal evolution of the core is given by

$$V_1\rho_1 c_{p1}\frac{\mathrm{d}T_1}{\mathrm{d}t} = Q_1 V_1 - F_1 a_1, \tag{1}$$

where V_1 is the volume of the core, ρ_1 is the density, c_{p1} is the isobaric specific heat capacity, $\mathrm{d}T_1$ is the change in temperature, $\mathrm{d}t$ is the time-step, Q_1 is the volumetric heat production, a_1 is the surface area and F_1 is the heat flow out of the core.

The heat flow out of the core is that conducted through the top thermal boundary layer, and is given by

$$F_1 = \frac{k_1(T_1 - T_{2b})}{\delta_{1t}}, \tag{2}$$

where k_1 is the core thermal conductivity, T_1 is the mean temperature, T_{2b} is the temperature at the base of the ice VI layer and δ_{1t} is the thickness of the top thermal boundary layer in the core.

Similar equations exist for the ice VI layer above the core. The thermal evolution of the ice VI layer is given by

$$V_2\rho_2 c_{p2}\frac{\mathrm{d}T_2}{\mathrm{d}t} = F_1 a_1 - F_2 a_2, \tag{3}$$

where V_2 is the volume of the ice VI layer, ρ_2 is the density, c_{p2} is the isobaric specific heat capacity, $\mathrm{d}T_2$ is the change in temperature, a_2 is the surface area and F_2 is the heat flow out of the ice VI layer.

The heat flow out of the ice VI layer is again controlled by the thickness of the top thermal boundary layer, and is given by

$$F_2 = \frac{k_2(T_2 - T_{3b})}{\delta_{2t}}, \tag{4}$$

where k_2 is the ice VI thermal conductivity, T_2 is the mean temperature, T_{3b} is the temperature at the base of the ocean and δ_{2t} is the thickness of the top thermal boundary layer in the ice VI layer.

Modeling the thermal evolution of the ocean is less trivial due to the release of latent heat as solids crystallize from solution during cooling. The composition of the crystallizate depends on the starting composition of the ocean; the initial ocean of aqueous ammonium sulfate lies in the water-rich part of the binary phase diagram (see Figs. 2 and 3 in Fortes et al., 2007), and therefore ice is the only crystallization product until the liquid composition reaches the eutectic (which we discuss later). Cooling of the ocean results in crystallization of ice I (at shallow levels), which, being less dense than the ocean, will float, thickening the crust (i.e. supra-oceanic ice shell) from below, and also ice VI (nearer the ocean floor), which being more dense than the ocean will sink, thickening the ice VI layer from above. In principle, this crystallization will continue to the eutectic where ice and ammonium sulfate will cocrystallize, or until all of the liquid has crystallized. For the sake of simplicity, we follow Grasset and Sotin (1996) in removing

Table 1
Parameters for thermal evolution calculations

Parameter	Symbol	Value	Units	Ref.
Planetary radius	r_4	2575	km	1
Surface temperature	T_s	95	K	1
Gravitational acceleration	g	1.37	$m\,s^{-2}$	1
Gas constant	R	8.3144	$J\,mol^{-1}\,K^{-1}$	
Initial crustal density	ρ_4	1065	$kg\,m^{-3}$	2
Ice I reference viscosity	$\eta_{0,icel}$	10^{12}	Pa s	3
Ice I activation energy	E_{icel}	60	$kJ\,mol^{-1}$	4
Ice I melting temperature	$T_{m,icel}$	273	K	5
Ice I density	ρ_{icel}	950	$kg\,m^{-3}$	4
Ice I latent heat	L_4	2.84×10^5	$K\,kg^{-1}$	6
Initial ocean radius	r_3	2452	km	2
Ocean density	ρ_3	1350	$kg\,m^{-3}$	2
Ice VI latent heat	L_2	2.94×10^5	$K\,kg^{-1}$	6
Ice VI reference viscosity	$\eta_{0,2}$	10^{12}	Pa s	3
Ice VI activation energy	E_2	136	$kJ\,mol^{-1}$	4
Ice VI melting temperature	T_{m2}	330	K	5
Initial ice VI radius	r_2	2299	km	2
Ice VI density	ρ_2	1400	$kg\,m^{-3}$	2
Core reference viscosity	$\eta_{0,1}$	10^{21}	Pa s	3
Core activation energy	E_1	525	$kJ\ mol^{-1}$	3
Core melting temperature	T_{m1}	1000	K	3
Core radius	r_1	1865	km	2
Core density	ρ_1	2750	$kg\,m^{-3}$	2

References: 1—Lodders and Fegley (1998); 2—Fortes et al. (2007); 3—Freeman (2006); 4—Durham and Stern (2001); 5—Bridgman (1937); 6—Kirk and Stevenson (1987).

the phase transitions from ice VI to ice V and ice V to ice III. The latent heat that is relevant to the ocean energy balance is that of ice VI (e.g., Grasset and Sotin, 1996), as any heat released will effectively flow down the thermal gradient into the cooler medium. Thus the thermal evolution of the ocean is given by

$$V_3\rho_3 c_{p3}\frac{dT_3}{dt} - \frac{dr_2}{dt}L_2\rho_2 4\pi r_2^2 = F_2 a_2 - F_3 a_3, \tag{5}$$

where V_3 is the volume of the ocean, ρ_3 is the density, c_{p3} is the isobaric specific heat capacity, dT_3 is the change in temperature, dr_2 is the change in radius at the bottom of the ocean, L_2 is the latent heat of crystallization for ice VI, r_2 is the radius at the bottom of the ocean, F_3 is the heat flow out of the ocean and a_3 is the surface area of the ocean.

Heat flow out of the ocean is governed by that extracted by the crust above, and is thus controlled by the thickness of the bottom thermal boundary layer in the crust. The heat flow out of the ocean is therefore given by

$$F_3 = \frac{k_4(T_{4b} - T_4)}{\delta_{4b}}, \tag{6}$$

where k_4 is the bulk crustal thermal conductivity, T_{4b} is the temperature at the base of the crust, T_4 is the mean crustal temperature and δ_{4b} is the thickness of the bottom thermal boundary layer in the crust.

The latent heat of ice I will in effect be incorporated into the crust (down the thermal gradient), and must therefore be considered in the energy balance for this layer, given by

$$V_4\rho_4 c_{p4}\frac{dT_4}{dt} + \frac{dr_3}{dt}L_4\rho_{icel}4\pi r_3^2 = F_3 a_3 - F_4 a_4 \tag{7}$$

where V_4 is the volume of the crust, ρ_4 is the density, c_{p4} is the isobaric specific heat capacity, dT_4 is the change in temperature, dr_3 is the change in radius at the top of the ocean, L_4 is the latent heat of crystallization for ice I, ρ_{icel} is the density of ice I, r_3 is the radius at the top of the ocean, a_4 is the planetary surface area and F_4 is the heat flow out of the ice VI layer.

The heat flow out of the crust is controlled by the thickness of the top thermal boundary layer, and is given by

$$F_4 = \frac{k_4(T_4 - T_s)}{\delta_{4t}}, \tag{8}$$

where k_4 is the bulk crustal thermal conductivity, T_s is the surface temperature and δ_{4b} is the thickness of the top thermal boundary layer in the crust.

The thickness of the thermal boundary layer in each case can be approximated by (Solomatov, 1995)

$$\delta = d/Nu, \tag{9}$$

where d is the thickness of the entire layer and Nu is the Nusselt number. The definition of the Nusselt number governs the parameterization of the heat flow equations via a simple relationship of general form

$$Nu = a\theta^b Ra^c \tag{10}$$

where the constants a, b and c depend on the stress dependence of viscosity and the convection regime in which the system is operating in; these being (i) small viscosity contrast regime, (ii) sluggish lid or transitional regime, or (iii) stagnant lid regime (e.g., Solomatov and Moresi, 2000). The Frank-Kamenetskii parameter, θ, is the natural logarithm of the viscosity contrast, given by

$$\theta = \frac{E\Delta T}{RT^2}, \tag{11}$$

where E is the activation energy, ΔT is the temperature contrast across the layer and R is the gas constant.

To investigate the effect that choice of scaling law may have on the ocean stability model we use two different parameterizations:

(i) a Newtonian scaling law for direct comparison with Grasset and Sotin (1996),

$$Nu = 0.294Ra^{0.3}. \tag{12}$$

(ii) a variable viscosity Newtonian stagnant lid scaling law (Moresi and Solomatov, 1995),

$$Nu = 1.89\theta^{-1.02}Ra^{0.2}. \tag{13}$$

We use a local Rayleigh number approach (e.g., Howard, 1964; Solomatov, 1995), in which the Rayleigh number, the ratio of buoyancy forces to viscous forces, is defined as follows,

$$Ra = \frac{\alpha g\rho\Delta T d^3}{\kappa\eta}, \tag{14}$$

where α is the thermal expansion, g is the acceleration due to gravity, κ is the thermal diffusivity (given by $\kappa = k/(\rho c_p)$) and η is the melting temperature-scaled viscosity at the local temperature defined as

$$\eta = \eta_0 \exp\left[l\left(\frac{T_m}{T} - 1\right)\right], \tag{15}$$

where η_0 is the viscosity of the material at the zero pressure melting point, T_m is the melting temperature and l is a constant given by

$$l = \frac{E}{RT_m}. \tag{16}$$

2.2. Temperature of the aqueous ammonium sulfate ocean

At the outset, the temperature of the ammonium sulfate ocean is controlled by the temperatures at its upper and lower margins. The temperature at the top of the ocean will always be at the melting temperature for ice I, whereas at the bottom of the ocean it will always be at the melting temperature for ice VI. The initial ocean temperature is taken as the mean of these two values, and changes by $\mathrm{d}T_3$ with every time-step $\mathrm{d}t$. We determine the temperature at the base of the ocean by using a linear fit to the melting curve of ice VI (Bridgman, 1937), given by

$$T_{3b} = 6.4346 \times 10^{-8} P_{3t} + 235.302, \tag{17}$$

where P_{3b} is the pressure at the base of the ocean due to the overlying layers. We also determine the temperature at the top of the ocean by using a linear fit to the melting curve of ice I (Bridgman, 1937), given by

$$T_{3t} = -1.05228 \times 10^{-7} P_{3b} + 274.354, \tag{18}$$

where P_{3t} is the pressure at the top of the ocean due to the overlying crust.

Knowledge of the melting curve of both ice I and VI as a function of pressure, and therefore radius, allows the rate of radius change for the top and bottom of the ocean to be determined. The gradient of the relevant melting curve is given by

$$s = \mathrm{d}T_m/\mathrm{d}r, \tag{19}$$

where $\mathrm{d}r$ is the change in radius. The difference in melting temperature at the top and bottom of the ocean must be accounted for when calculating the change in radius that accompanies a change in ocean temperature (Fig. 2). Incorporating the gradient of both the melting curve and adiabat allows us to determine the radius change at the bottom and top of the ocean as follows,

$$\mathrm{d}r_2 = \frac{\mathrm{d}T_3}{(s_2 - s_{\mathrm{ad}})}, \tag{20}$$

$$\mathrm{d}r_3 = \frac{\mathrm{d}T_3}{(s_3 + s_{\mathrm{ad}})}, \tag{21}$$

where s_{ad} is the adiabatic gradient in the ocean ($=(T_{m3} - T_{m2})/d_3$) and s_2 and s_3 are the gradients of the melting curves at the bottom (ice VI) and top (ice I) of the ocean. We can then substitute for $\mathrm{d}r_2$ in Eq. (5) to determine the temperature evolution of the ocean and solve Eq. (21) to determine the radius change at the top of the ocean for use in Eq. (7).

2.3. Crustal properties

The bulk thermophysical properties of the crust must be specified in order to calculate the heat flux through the crust. The crust is assumed to be composed predominantly of methane clathrate, with some ice Ih and ammonium sulfate derived from the primitive ocean by intrusion of the original crust (cf. Fortes et al., 2007).

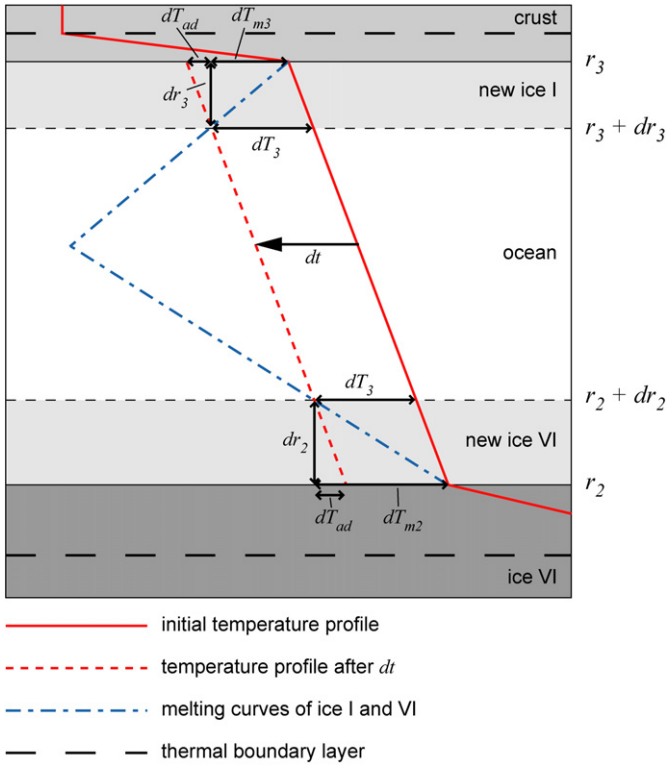

Fig. 2. Schematic diagram showing cooling of the ocean. The ocean has an initial temperature profile governed at the top and bottom by the melting temperature of ice Ih and ice VI respectively. We assume a linear adiabat joining these two temperatures. During the time-step $\mathrm{d}t$, the ocean cools by the amount $\mathrm{d}T_3$ to give a new temperature profile. Knowing the melting curves of ice Ih and ice VI allows us to determine the accompanying change in radius. In each case we must allow for the adiabatic component ($\mathrm{d}T_{\mathrm{ad}}$) in the temperature change.

We assume that the small quantities of ammonium sulfate have a negligible effect on the bulk crustal properties over the entire evolution. We allow for crustal underplating by ice Ih by using a weighting scheme for the bulk properties of the crust over time.

Unlike most crystalline materials, the thermal conductivity of the methane clathrate in the crust increases with increasing temperature, behavior more typical of amorphous solids. We allow the thermal conductivity of the methane clathrate to change according to the experimental data of Krivchikov et al. (2005) (Fig. 3a), which is given by

$$k_{\mathrm{clath}} = 0.498 - 2.30T^{-1} + 4.708T^{-2} - 3.718T^{-3}. \tag{22}$$

The thermal conductivity of ice decreases with increasing temperature and can be estimated by fitting a 9th order polynomial (Ross and Kargel, 1998) to previous experimental data (Klinger, 1973; Ross et al., 1977; Slack, 1980; Andersson and Suga, 1994) (Fig. 3a),

$$k_{\mathrm{icel}} = M_0 + M_1 \log T + M_2 \log T^2 + \cdots M_n \log T^n, \tag{23}$$

where the variables M_0 to M_n are given by Ross and Kargel (1998).

We then use a weighting scheme to estimate the thermal conductivity of a heterogeneous crust, which depends on the volume fraction of methane clathrate (x_{clath}) and ice Ih present in the crust (Fig. 3b),

$$k_4 = x_{\mathrm{clath}} k_{\mathrm{clath}}(T) + (1 - x_{\mathrm{clath}}) k_{\mathrm{icel}}(T). \tag{24}$$

The thermal expansivity of methane clathrate can also be estimated as a function of temperature. We do this by fitting a polynomial to the experimental data of Shpakov et al. (1998) (Fig. 4a),

$$\alpha_{\mathrm{clath}} = 2.09 \times 10^{-9} T + 3.7 \times 10^{-8}. \tag{25}$$

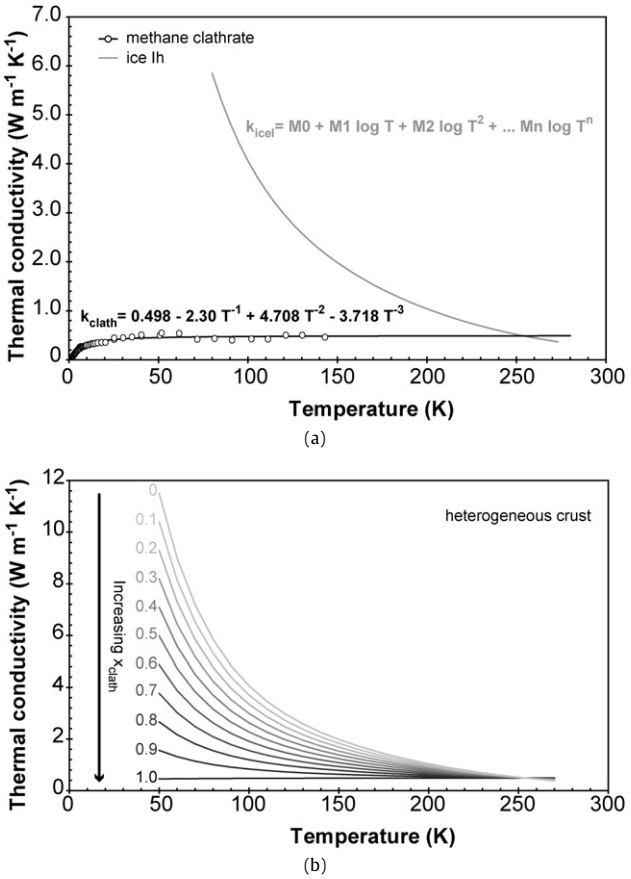

Fig. 3. Thermal conductivity from experimental data. (a) Methane clathrate data from Krivchikov et al. (2005); ice Ih curve fitted by Ross and Kargel (1998) to data from Klinger (1973), Ross et al. (1977), Slack (1980), and Andersson and Suga (1994). In each case the polynomial fit to the data is given. (b) The thermal conductivity of a heterogeneous crust made of x_{clath} fraction of methane clathrate, determined from Eq. (24).

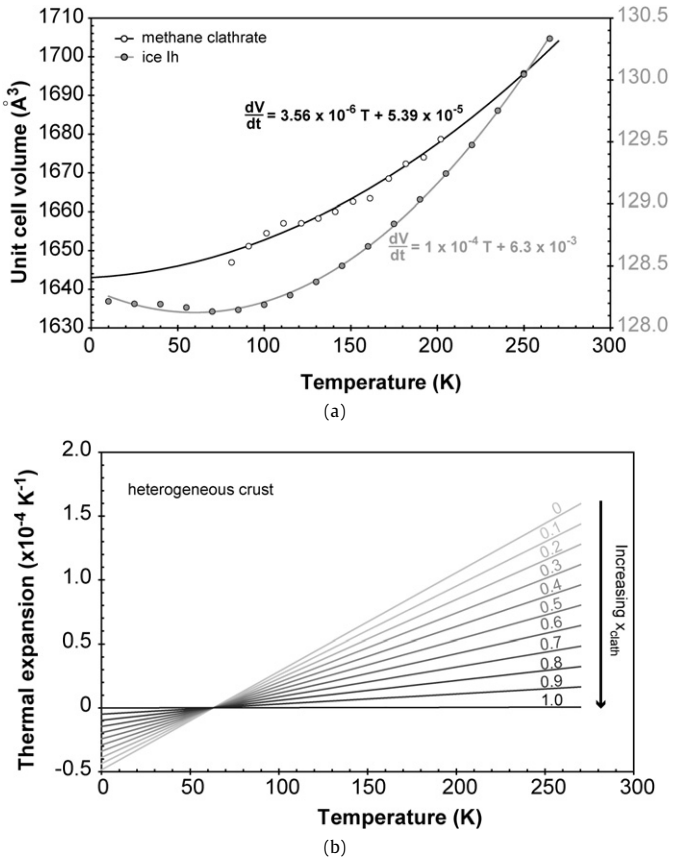

Fig. 4. Thermal expansion from experimental data. (a) Methane clathrate data from Shpakov et al. (1998); ice Ih data from Röttger et al. (1994). In each case the first derivative of the volume as a function of temperature (dV/dT) is given, which is used in the equation $\alpha = (1/V)(dV/dT)$ to determine the bulk thermal expansion. (b) The thermal expansion of a heterogeneous crust made of x_{clath} fraction of methane clathrate, determined from Eq. (27).

We determine the thermal expansivity of ice Ih by fitting a polynomial to the experimental data of Röttger et al. (1994) (Fig. 4a),

$$\alpha_{\text{icel}} = 7.71 \times 10^{-7} T - 4.85 \times 10^{-5}. \tag{26}$$

Although this polynomial does not fit the data well at low temperatures, it is satisfactory at the warmer temperatures we are interested in here. We again use a weighting scheme to estimate the thermal expansivity of a heterogeneous crust (Fig. 4b),

$$\alpha_4 = x_{\text{clath}}\alpha_{\text{clath}}(T) + (1 - x_{\text{clath}})\alpha_{\text{icel}}(T). \tag{27}$$

The specific heat capacity of methane clathrate has been measured by Handa (1986) in the temperature range 85 to 270 K (Fig. 5a), to which we fit a 3rd order polynomial,

$$c_{p,\text{clath}} = 4.971 \times 10^{-5} T^3 - 0.0289 T^2 + 11.66 T + 55.92. \tag{28}$$

We estimate the specific heat capacity of ice by fitting a 3rd order polynomial to the experimental data of Giauque and Stout (1936), conducted in the temperature range 16 to 268 K (Fig. 5a),

$$c_{p,\text{icel}} = 7.57 \times 10^{-5} T^3 - 0.0389 T^2 + 13.26 T - 136.6. \tag{29}$$

We use a similar weighting scheme to that above to estimate the specific heat capacity of a heterogeneous crust (Fig. 5b),

$$c_{p,4} = x_{\text{clath}} c_{p,\text{clath}}(T) + (1 - x_{\text{clath}}) c_{p,\text{ice}} I(T). \tag{30}$$

The density of the crust is also allowed to change with time as a result of the underplating by ice Ih by a similar weighting scheme,

$$\rho_4 = x_{\text{clath}}\rho_{\text{clath}} + (1 - x_{\text{clath}})\rho_{\text{icel}}. \tag{31}$$

The bulk viscosity of the crust is also determined using a weighting scheme. Although the rheology of methane clathrate under conditions we wish to model is not known well, it is probably significantly stronger than ice Ih (Durham et al., 2003). Therefore we assume that the viscosity of methane clathrate is 20 times that of ice Ih (Durham et al., 2003), and that the bulk viscosity of the crust can be given by

$$\eta_4 = x_{\text{clath}}\eta_{\text{clath}} + (1 - x_{\text{clath}})\eta_{\text{icel}}. \tag{32}$$

Note that we employ a melting temperature-scaled relationship for the viscosity of each layer (i.e. contours of constant viscosity are approximately parallel to the melting curves for the material of each layer), when in reality the strain rate (and hence effective viscosity) is likely to be a function of stress, grain size and activation energy (see review by Durham and Stern, 2001, for ice). These governing parameters are incorporated into the *Ra–Nu* scaling laws for non-Newtonian rheologies, but to investigate the sensitivity of the model for our Newtonian cases, we vary the reference viscosity between 10^{11} and 10^{14} Pa s.

2.4. Core and ice VI properties

The only source of heat that we consider is that due to the decay of radioactive nuclides in the silicate layer. The implication of this assumption is discussed later. The heat production is represented as the sum of heat produced for each of the radioactive

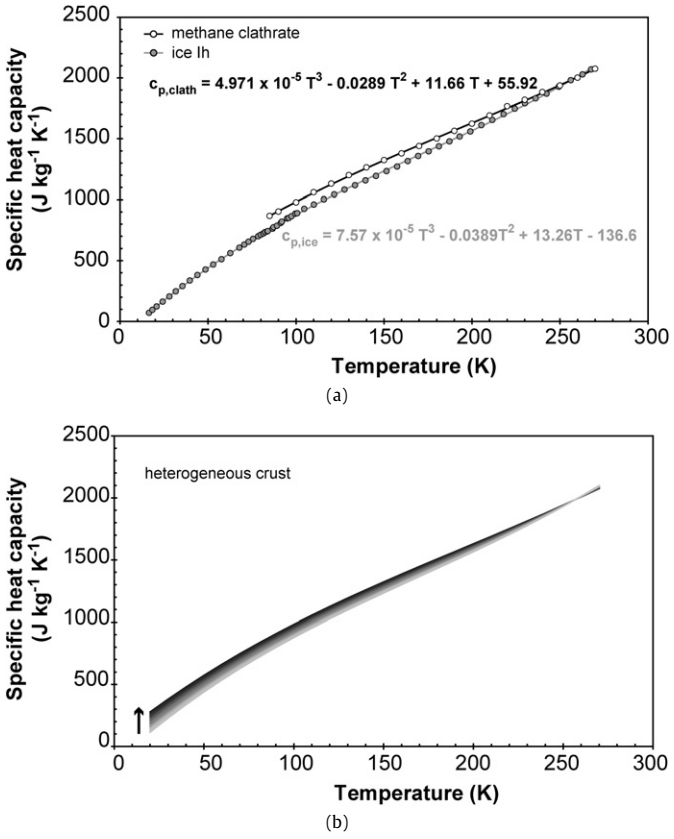

Fig. 5. Specific heat capacity from experimental data. (a) Methane clathrate data from Handa (1986); ice Ih data from Giauque and Stout (1936). In each case the polynomial fit to the data is given. (b) The specific heat capacity of a heterogeneous crust made of x_{clath} fraction of methane clathrate, determined from Eq. (30). The arrow shows the curves for increasing x_{clath}, which reverses at ~250 K.

species ^{235}U, ^{238}U, ^{232}Th and ^{40}K, and is given by (Turcotte and Schubert, 2002)

$$Q(t) = \sum_{i=1}^{n} Q_i A_i \exp(-\lambda_i t), \tag{33}$$

where Q_i is the heat production rate of species i at time, A_i is the initial abundance of species i, given by Turcotte and Schubert (2002), and λ_i is the decay constant of species i. To investigate the possible uncertainty in the abundances of heat producing elements in the silicate core, we consider two different compositions which are described in more detail in a later section.

The starting model (Fortes et al., 2007) assumes complete hydration of the silicate core to the serpentine mineral antigorite (13 wt% H_2O). The thermal conductivity of serpentinite group minerals as a function of temperature has been previously investigated experimentally. We have fitted the thermal conductivity data for antigorite of Seipold and Schilling (2003) over the range 300–1000 K (Fig. 6a). Note that we ignore the likely dehydration of antigorite at 850–900 K in high-PT water-saturated systems, so the thermal conductivity is given by

$$k_1 = \frac{1}{0.404 + 0.000246T}. \tag{34}$$

The thermal expansivity of antigorite as a function of temperature has not been investigated experimentally, and therefore we use the mineral chlorite as an analogue, taking a linear fit to the data of Pawley et al. (2002) (Fig. 6b),

$$\alpha_1 = 4.998 \times 10^{-9} T + 1.057 \times 10^{-7}. \tag{35}$$

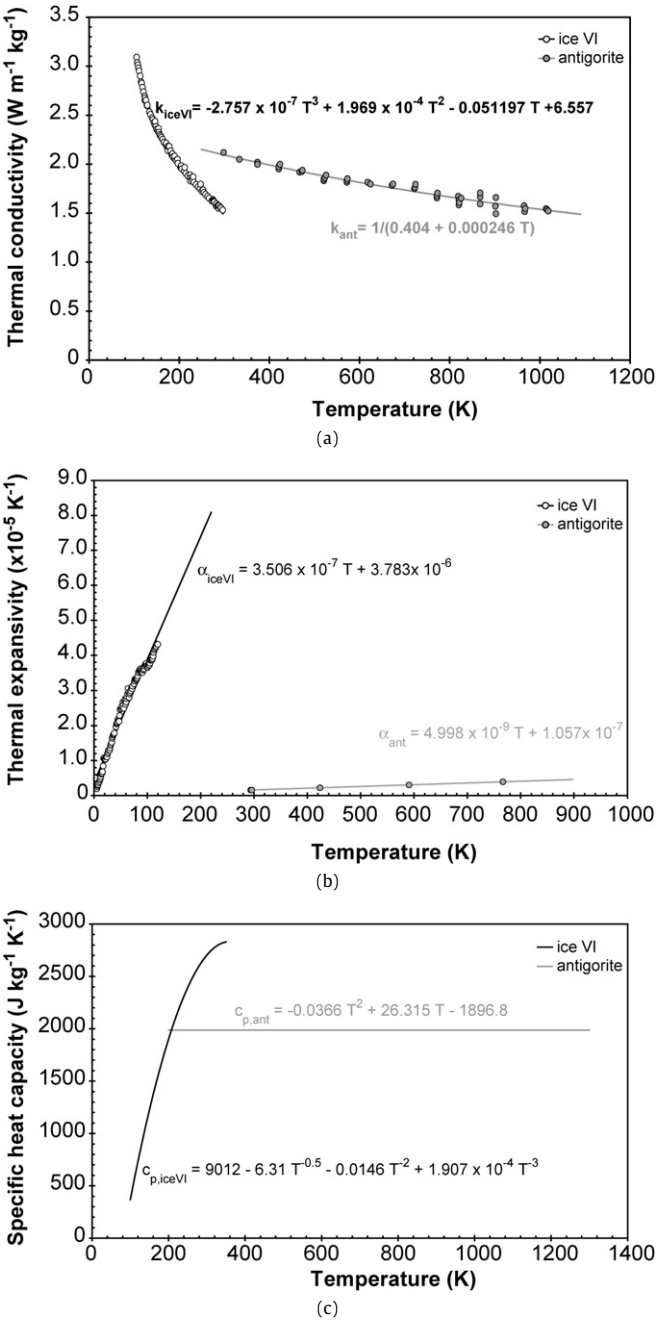

Fig. 6. Temperature-dependent properties of the antigorite core and ice VI shell from experimental data. (a) Thermal conductivity data for antigorite from Seipold and Schilling (2003), determined from Eq. (34); thermal conductivity data for ice VI from Ross et al. (1978), determined from Eq. (37), (b) thermal expansivity data for chlorite analogue from Pawley et al. (2002), determined from Eq. (35); thermal expansivity data for ice VI from Mishima et al. (1978), determined from Eq. (38), and (c) specific heat capacity of antigorite determined from Berman and Brown (1985), determined from Eq. (36); specific heat capacity data for ice VI from Tchijov (2004), determined from Eq. (39).

The heat capacity of the antigorite core can be estimated as a function of temperature, and is of the general form (Fig. 6c)

$$c_{p,1} = k_a + k_b T^{-0.5} + k_c T^{-2} + k_d T^{-3} \tag{36}$$

where k_a, k_b, k_c and k_d are mineral-specific parameters, which for antigorite are 9012 $\mathrm{J\,K^{-1}\,mol^{-1}}$, −6.31 $\mathrm{J\,K^{-1/2}\,mol^{-1}}$, −0.0146 $\mathrm{J\,K\,mol^{-1}}$, and 1.907×10^{-4} $\mathrm{J\,K^2\,mol^{-1}}$ (Berman and Brown, 1985). This value for heat capacity is then converted into J kg^{-1} by dividing by the molecular weight of antigorite given by the chemical formula in Berman and Brown (1985).

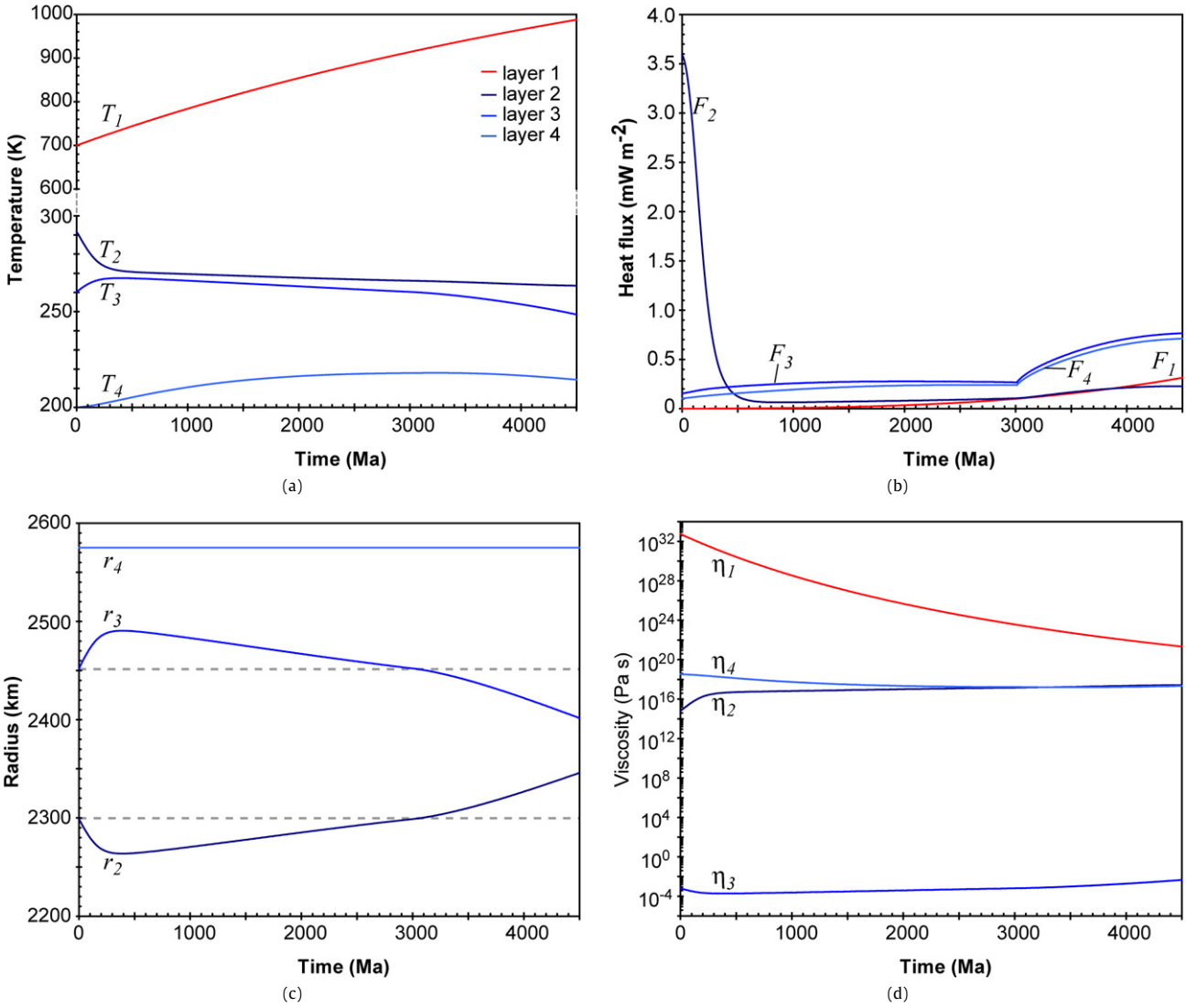

Fig. 7. Results of the nominal model, showing some of the typical outputs for a given run. (a) Mean temperature of layer 1 (core—T_1), layer 2 (ice VI—T_2), layer 3 (ocean—T_3) and layer 4 (crust—T_4); (b) heat flux out of core (F_1), ice VI layer (F_2), ocean (F_3) and crust (F_4); (c) radius of bottom ocean boundary (r_2), top ocean boundary (r_3) and surface (r_4); (d) mean viscosity of core (η_1), ice VI layer (η_2), ocean (η_3) and crust (η_4). The viscosity of the ocean is not used in the thermal evolution models but is included here for reference.

In a similar manner to the crust and core, we use experimental data to more accurately model the parameters of the ice VI shell. We estimate the thermal conductivity of the ice VI shell by fitting a 3rd order polynomial to the experimental data of Ross et al. (1978) (Fig. 6a),

$$k_2 = -2.757 \times 10^{-7} T^3 + 1.969 \times 10^{-4} T^2 - 0.05119T + 6.557. \quad (37)$$

The limited data on the thermal expansion of ice VI as a function of temperature suggest a linear fit is sufficient Mishima et al. (1978) (Fig. 6b),

$$\alpha_2 = 3.506 \times 10^{-7} T + 3.783 \times 10^{-6}. \quad (38)$$

We fit a 2nd order polynomial to the equation of state derived specific heat capacity for ice VI at 1.0 GPa given by (Tchijov, 2004; Fig. 6c)

$$c_{p,2} = -0.0366T^2 + 26.315T - 1896.8. \quad (39)$$

3. Results

In order to determine the long-term stability of an aqueous ammonium sulfate ocean on Titan, we perform a parameter space study of likely conditions. Of particular importance are the influence of initial core temperature and heat production rate, different *Ra–Nu* scaling laws and the effect of a heterogeneous crust with a time-variable composition. We begin by describing the nominal model as a basis for comparison with the parameter space investigated, and then summarize the effects of varying initial conditions, rheologies and crustal compositions.

3.1. Nominal thermal model

Although there is uncertainty in the correct formulation of our nominal model, it does use current thinking about Titan as a benchmark to explore possible differences later on. In this model we assume that the core has an abundance of heat-producing isotopes similar to the mean terrestrial mantle composition, given by Turcotte and Schubert (2002). The model has a variable Newtonian viscosity (Eq. (15)) throughout, with a reference viscosity of 10^{12} Pa s. We use initial core and crustal temperatures of 700 and 200 K respectively and allow the model to run for 4.5 Ga, using the stagnant lid scaling law (Eq. (13)).

Fig. 7 shows the basic results and features of the nominal model. The temperature in the core (Fig. 7a) increases to almost

990 K as a result of the heat generated by the radioactive isotopes. This is probably sufficient to cause core dehydration. The ice VI layer cools rapidly for the first ~500 Ma, approaching the temperature of the ocean above, but cools at a much slower rate for the next 4 Ga, decreasing in temperature by ~5 K over this time period. The ocean warms rapidly by about 7 K during the first ~500 Ma, due to the heat flux from the ice VI below, after which it cools by ~20 K over the remaining 4 Ga. The crust warms gradually by about 20 K during the first 3.3 Ga, after which it cools by 4 K. The heat flux from each layer (Fig. 7b) directly influences the temperature of that layer. The heat flux from the core increases from zero at the outset to a maximum of about 0.3 mW m^{-2} at 4.5 Ga, as a result of the radiogenic heating in this layer. The ice VI layer has a high initial heat flow of ~3.5 mW m^{-2} which decreases to almost zero by about 500 Ma, and then remains fairly constant until 3 Ga when it increases again as a result of the transfer of radiogenic heat from the core. The heat flux out of the ocean and the crust are similar as they are both governed to a large extent by the bulk properties of the crust. Both heat fluxes increase to almost 0.3 mW m^{-2} until about 3 Ga, where both show a sudden increase as a result of the beginning of crustal underplating by ice I. The radii of the top and bottom of the ocean (Fig. 7c) are controlled not only by the ocean heat fluxes, but also by the generation of latent heat and the melting curves of ice Ih and ice VI. The ocean initially grows in size as a result of its warming during the first 500 Ma, after which crystallization begins at a steady rate. This steady rate of ocean reduction continues until about 3 Ga where the ocean begins to crystallize at a quicker rate as a result of the ice underplating. The final ocean thickness is about 56 km, leaving a crust of 173 km thickness above, of which the bottom 50 km is expected to be ice Ih. The pressure at the bottom of this crust (~245 MPa) is probably high enough to form a layer of ice II. The viscosity of each layer (Fig. 7d) reflects the difference between the mean layer temperature and the reference melting temperature for that layer: viscosity follows increases and decreases in the temperature difference closely, with the core showing the greatest temperature, and therefore viscosity, change. Thus for the nominal model, the ammonium sulfate ocean survives to the present day, albeit with a reduced thickness.

3.2. Effect of different Ra–Nu scaling laws

The main effect of changing from a variable viscosity Newtonian stagnant lid scaling law (Eq. (13); Moresi and Solomatov, 1995) to a simple scaling law (Eq. (12); Grasset and Sotin, 1996) is on the rate of heat transfer (Fig. 8a). The efficiency of this heat transfer depends largely on the exponential constant c for the Rayleigh number, which is smaller for the variable viscosity Newtonian stagnant lid scaling law. For the simple scaling law, the core temperature rises to 960 K, but the heat flux rises significantly from about 1 Ga to just over 3 mW m^{-2}. The initial heat flux out of the ice VI layer is very similar to that of the nominal scaling law, but shows a significant increase from about 2 Ga due to heating from the core below, with a final heat flux of almost 2 mW m^{-2}. Initial heat fluxes for the ocean and crust are slightly larger, but decrease gradually until about 4 Ga, where the heat flux from the ice VI begins to have an influence. The effect of the different heat flux transfer on the stability of the ocean is shown in Fig. 8b. After a similar initial period of melting, the ocean thickness remains almost constant until about 3 Ga, where the heat flux from the ice VI begins to warm the ocean, causing melting. This melting continues throughout the remainder of the model, leaving an ocean of final thickness of about 376 km, and a crust about 6 km thick above.

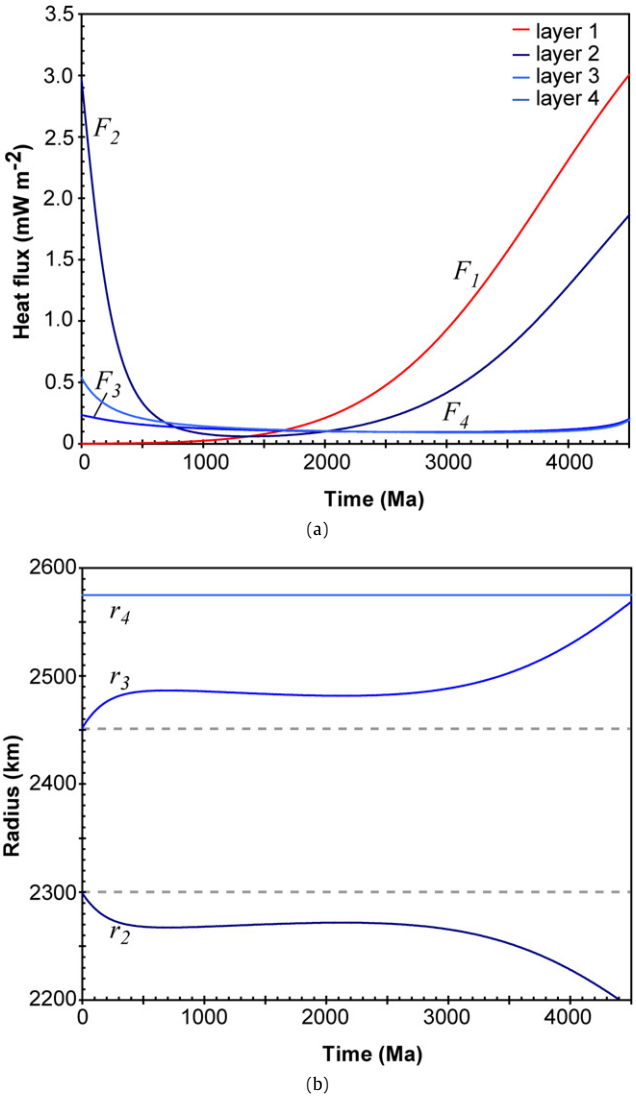

Fig. 8. Effect of changing the *Nu–Ra* scaling law, for comparison with the nominal model in Fig. 7. (a) Heat flux out of core (F_1), ice VI layer (F_2), ocean (F_3) and crust (F_4); (b) radius of bottom ocean boundary (r_2), top ocean boundary (r_3) and surface (r_4).

3.3. Effect of variations in heat production

The main effect on our model of changing the rock composition is from the change in the amount of radiogenic heat produced. We considered the effect of changing the concentrations of ^{235}U, ^{238}U, ^{232}Th and ^{40}K to those more typical of chondritic material. The average chondritic concentrations of uranium and thorium are a factor of 4 less than in our nominal model, whereas that of potassium is larger by a factor of 2 (Turcotte and Schubert, 2002). Using these concentrations changes the heat production rate only slightly, decreasing the final volumetric heat production rate in the core by about a third. The decrease in the amount of heat transferred to the ocean results in an increased cooling rate, although for the nominal model the ocean survives, albeit at about half the nominal thickness at 28 km (Fig. 9a). The crustal thickness increases only by a factor of about a third (14 km) with the chondritic core model, as crystallization only occurs at one boundary for this layer. We do not consider the effect of Al^{26} as a heat source, as it is likely more important in the early history of small icy bodies (e.g., Prialnik and Bar-Nun, 1990; Castillo-Rogez, 2006), rather than throughout the evolution of large

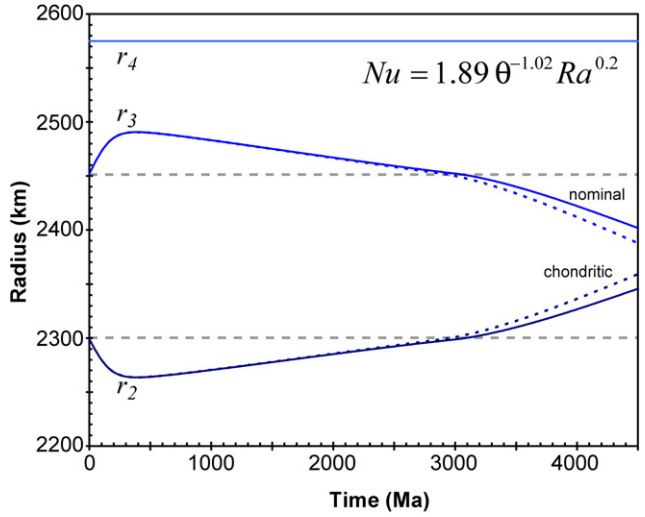

(a)

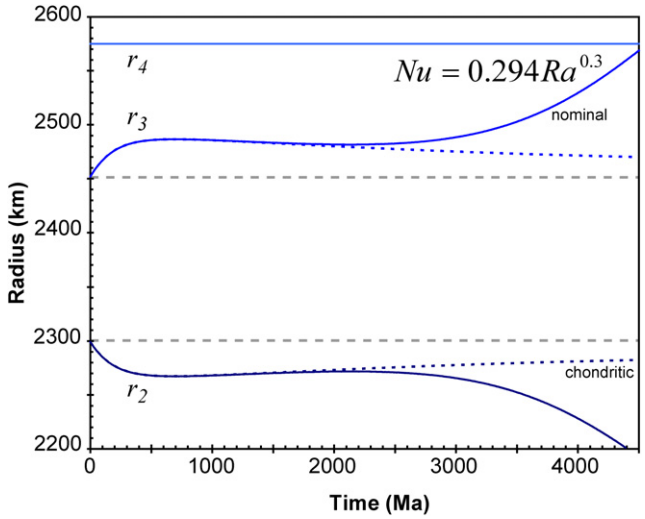

(b)

Fig. 9. Effect of changing the concentration of heat-producing elements in the core, for comparison with the nominal model in Fig. 7. (a) Layer boundaries for the nominal (solid lines) and chondritic (dashed lines) models, using the stagnant lid scaling law. (b) Layer boundaries for the nominal (solid lines) and chondritic (dashed lines) models, using the simple isoviscous scaling law.

icy bodies such as Titan. The effect of a chondritic core when using the simple isoviscous scaling law is shown in Fig. 9b. The decrease in heat flux in this case makes the ocean more stable to melt through, reducing the ocean thickness to 105 km, leaving a crust 188 km thick above.

3.4. Effect of changing core and ice properties

We also wished to investigate the effect of using realistic material properties derived from experimental data for the rock and ice layers. Fig. 10 shows the evolution of thermal conductivity, expansivity, specific heat capacity and density for each of the solid layers for the nominal model. The thermal conductivities of the antigorite and ice VI layers follow the inverse of their temperatures, showing a decrease and increase in conductivity respectively (Fig. 10a). The thermal conductivity of the crust is initially almost an order of magnitude smaller than for the other solid layers, as a result of the bulk crustal composition being dominated by methane clathrate. The addition of ice Ih to the base of the crust from about 3 Ga results in an increase in the crustal thermal conductivity of about 80% over the remaining 1.5 Ga. The thermal expansivity of the crust follows a similar trend (Fig. 10b), but increases by two orders of magnitude from 3 Ga. The expansivity of the ice VI varies by a similar amount to the conductivity, but in the opposite direction, and remains an order of magnitude larger than the antigorite expansivity, which changes little during the entire evolution. The specific heat capacities of all three layers (Fig. 10c) have the most similar values of all the material properties. The heat capacity of the antigorite core varies negligibly, whereas the ice VI and crustal layers follow similar trends to their temperatures, ending at about 2040 and 1705 $J\,m^{-1}\,K^{-1}$ respectively. Fig. 10d shows the effect of using a bulk weighting scheme for the crust, the density of which depends on the mass of ice Ih crystallized at its base. The density of the crust decreases by 3% after ice Ih is added from 3 Ga, which is now made of ~72% methane clathrate and 28% ice Ih.

3.5. Effect of initial temperatures

The initial temperatures of the ocean and ice VI layer are not free parameters, and are instead defined as the mean of the melting temperatures at the top and bottom of each respective layer. We are therefore limited to changing the initial core and crustal temperatures only, which can still have a significant effect. Figs. 11a and 11b show the thickness of the ocean, or the time at which it freezes, for different initial core and crustal temperatures respectively, for the nominal scaling law (Eq. (13)). Simply stated, the hotter the initial core temperature the thicker the final ocean. An initial core temperature of 500 K results in an ocean of 190 km thickness, whereas an initial core temperature of 900 K results in an ocean 355 km thick. A reverse situation exists for the crustal temperature, where the ocean survives for longer if the crust is initially cool. An initial crustal temperature of 100 K results in an ocean thickness of 264 km, whereas an initial crustal temperature of 240 K results in the ocean freezing by about 3.7 Ga. Figs. 11c and 11d show identical plots for the simple scaling law (Eq. (12)). There exist similar relationships between ocean thickness and initial temperatures, but under this scaling law the ocean persists under all initial conditions, and actually melts through the crust for initial core temperatures above about 700 K and below initial crustal temperatures of about 175 K.

To fully investigate the role of initial core and crustal temperatures we have conducted a parameter space survey for 4 magnitudes of ice reference viscosity (Fig. 12). These plots show that at lower viscosities the persistence, and thickness, of the ocean is more sensitive to the initial crustal and core temperatures than at higher viscosities. Several key features can be observed in Fig. 12. Generally, at low core temperatures, the crustal temperature is more important, whereas at high core temperatures, this situation is reversed. There is a noticeable tightening of the contour lines at warm core and crust temperatures in the lowest two viscosities, as a result of the underplating of ice I changing the bulk properties of the crust significantly. There is also a noticeable kink in the contours at the warmest core and lowest crust temperatures; this is the result of an unrealistically thin crust ($\sim$ <1 km) being able to transfer heat very effectively, and thus resisting complete melt through where it would otherwise be expected. These contours then flow into the region of melt through in each viscosity case, with the largest number of melt through models occurring at the highest viscosities. It is also evident that the optimum conditions for survival of the ocean are a warm core and cold crust, and that for the largest two reference viscosities, the ocean does not freeze for any studied initial core and crust temperature.

4. Discussion

The most important result of this study is that an ocean of aqueous ammonium sulfate can remain liquid inside Titan, to the

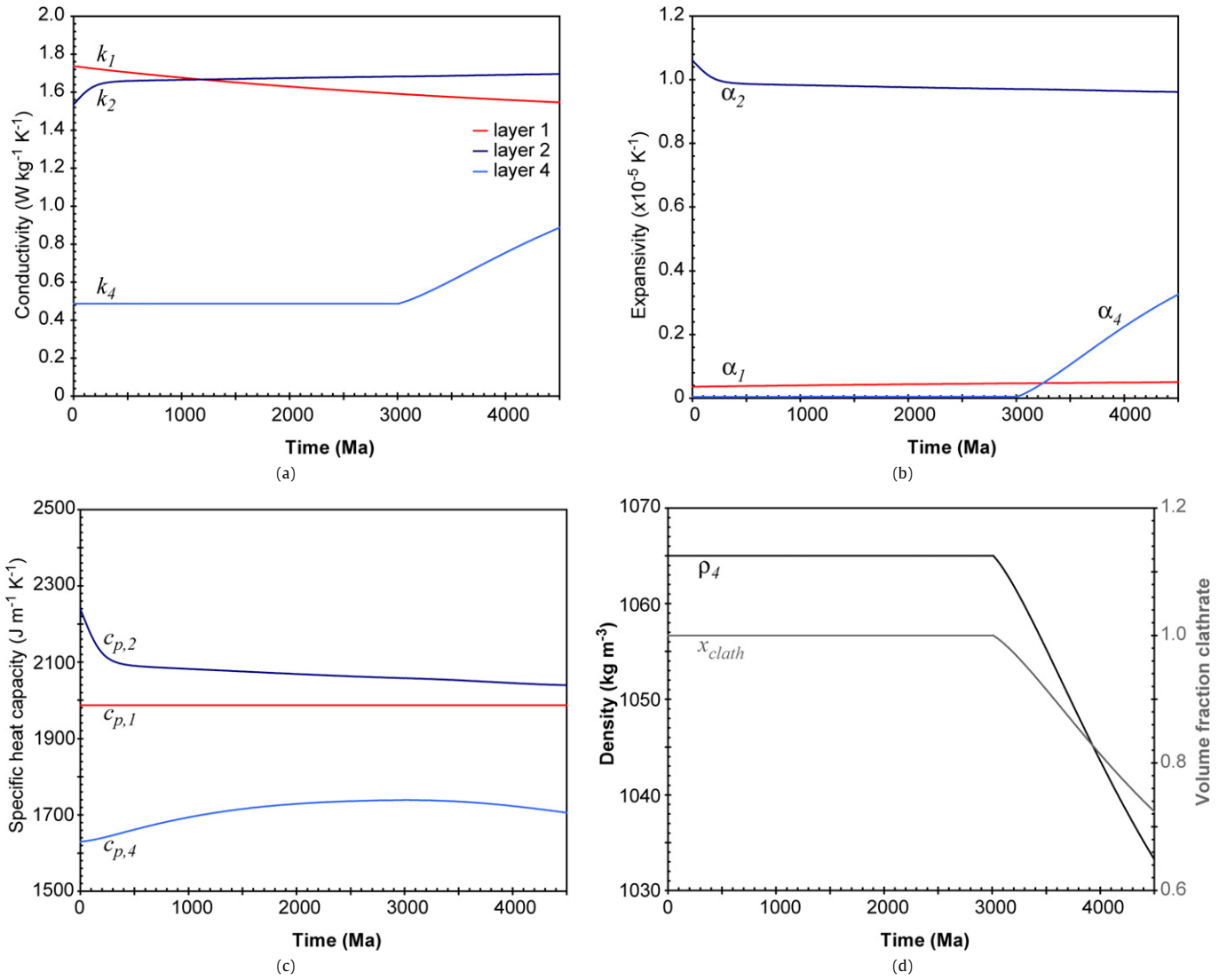

Fig. 10. Core and ice material properties over the evolution of the nominal model. (a) Mean thermal conductivity of layer 1 (core—k_1), layer 2 (ice VI—k_2) and layer 4 (crust—k_4); (b) thermal expansivity of core (α_1), ice VI layer (α_2) and crust (α_4); (c) specific heat capacity of core ($c_{p,1}$), ice VI layer ($c_{p,2}$) and crust ($c_{p,4}$); (d) density of the heterogeneous crust (ρ_4) and the methane clathrate mass fraction (x_{clath}).

present day, under a wide range conditions. To assess the validity and importance of this we first discuss the nominal model parameters and assumptions, paying particular attention to rheology and convection, and then discuss the implications for Titan's evolution.

4.1. Constraining the nominal model

The initial conditions of our thermal evolution model are governed to a certain extent by the chemical model predicted by Fortes et al. (2007). The formation of a hydrated core of antigorite requires temperatures of less than about 900 K, and therefore we assume that the initial temperature of the core must have fulfilled this requirement. As a result of the radiogenic heat produced within this layer, the temperature of the core increases by several hundred degrees over 4.5 Ga in all models. In the nominal model, the final core temperature is ~990 K, meaning that the antigorite would have most likely dehydrated to forsterite and enstatite, plus 28% water by volume. This could lead to a change in the bulk core properties, and the liberated superheated water would percolate upwards, where it may freeze to ice VII in the cooler outer part of the core, or as ice VI in the ice shell. It is interesting to note that this dehydration process is endothermic (Robie and Hemingway, 1995), and that warming of the core through this boundary, and subsequent change in the bulk properties, is buffered by the dehydration reaction. The process of rising and cooling water in the high pressure ice phase was assumed by Grasset and Sotin (1996) to be responsible for this layer being at its melting temperature at every depth, which we do not observe in our model due to the high pressures (~1.3 GPa at its base). The crustal temperature is constrained at its surface by the known surface temperature on Titan (assuming it has remained constant over its evolution) and at its base by the melting temperature of ice I at a given pressure. The temperature gradient through the crust, and thus the mean temperature of the layer, is governed by the heat loss mechanism present. If the crust is convecting (which we discuss below), then we would expect a fairly constant temperature through the majority of the crust, with large and small thermal boundary layers at the top and bottom respectively.

Our thermal evolution model assumes convective heat transfer in each layer throughout the entire evolution. To assess the likelihood of this assumption we monitor the Rayleigh number as a function of time. Convection is possible when the Rayleigh number is greater than some critical Rayleigh number, which is typically of the order of about 500 (e.g., Nimmo and Stevenson, 2000). In the nominal model (Fig. 13a), the ice VI layer Rayleigh

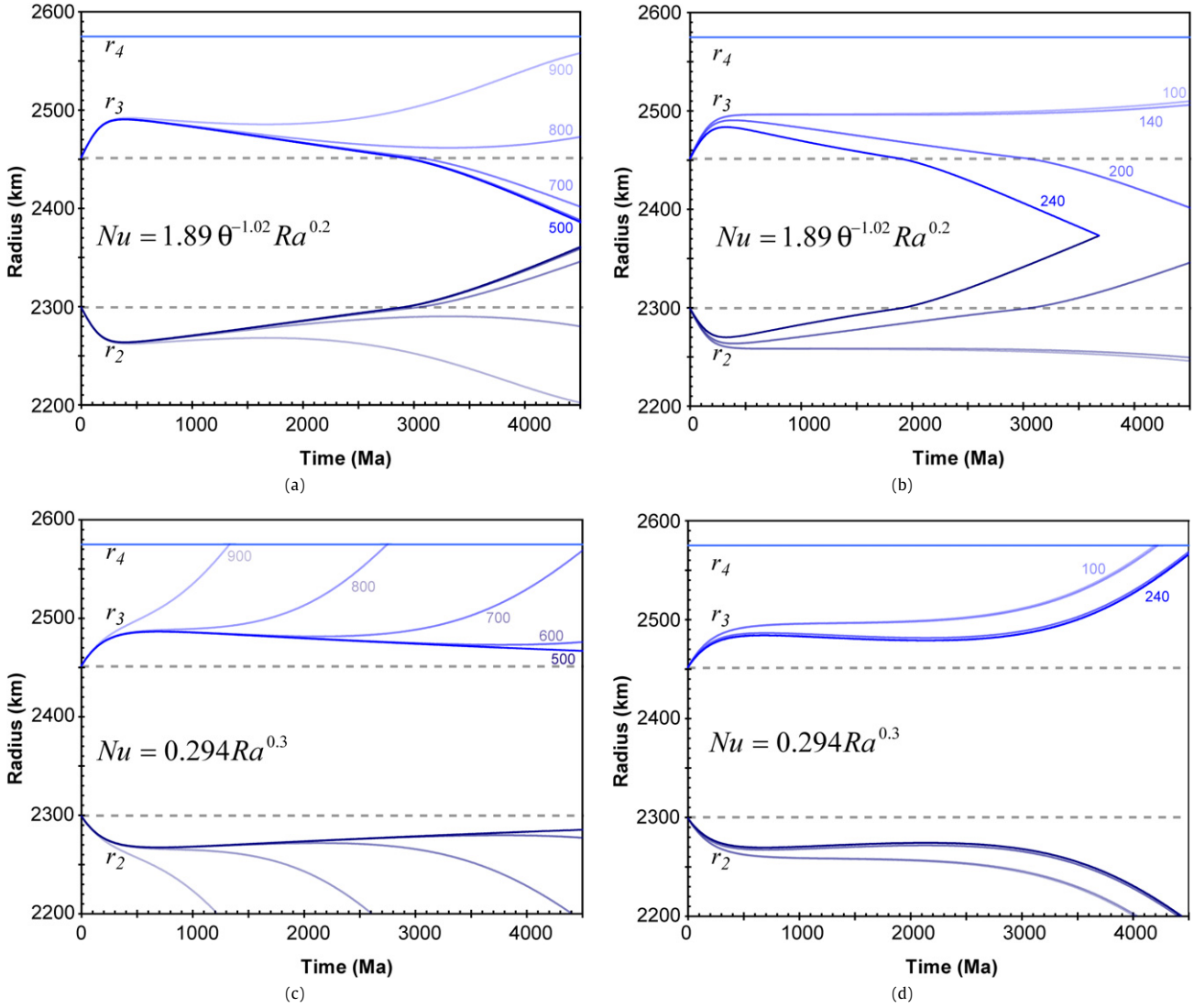

Fig. 11. Effect of initial temperatures on the persistence of the ocean for different scaling laws. For stagnant lid scaling law, radii of ocean boundaries for different initial core temperatures in K (a) and different initial crustal temperatures in K (b). For simple isoviscous scaling law, radii of ocean boundaries for different initial core temperatures in K (c) and different initial crustal temperatures in K (d). All other parameters are the same as in the nominal case.

number is super-critical at all times, as its temperature is close to its melting temperature. The crustal Rayleigh number becomes and remains super-critical after 1.1 Ga, whereas the core does not begin convecting until about 3 Ga. If the initial core temperature is increased (Fig. 13b), whilst holding all other parameters the same as the nominal model, the core begins convecting after 120 Ma, the ice VI layer does not change significantly, and the crust begins to convect at the same time as before, but this time becomes sub-critical for the last 800 Ma as a result of significant crustal thinning. However, the likelihood (and efficiency) of convection cannot be determined from the Rayleigh number alone. A recent study showed that Newtonian stagnant-lid convection may continue even after the Rayleigh number is sub-critical (Solomatov and Barr, 2006), indicating that a convective regime might still be a valid assumption even under these conditions. It has also been shown that when the Rayleigh number is just greater than the critical Rayleigh number, a steady-state convection regime is applicable. This regime has a heat flow that is less efficient than a time-dependent regime ($Ra \gg Ra_c$), due to a change in the exponential factor in the *Ra*–*Nu* scaling law (e.g., Hauck and Phillips, 2002; McKinnon, 2006). Our nominal scaling law effectively assumes a steady-state regime, and therefore any change to a time-dependent regime would increase the heat flux from each layer. It has also been shown that the onset of convection in a non-Newtonian fluid requires a large amplitude perturbation, whereas for Newtonian rheologies (as assumed here) only small perturbations are required (Barr et al., 2004; Barr and Pappalardo, 2005). Recently, McKinnon (2006) presented a strong case for Newtonian convection occurring in the outer ice I shell of Callisto, and by extrapolation, also of Ganymede and Titan. Therefore we feel that the assumption of a Newtonian stagnant-lid convective regime in the ice layers is reasonable.

In reality, when convection is not occurring in a layer, heat will be transferred by diffusion, and so the effect of neglecting this heat transfer mechanism is to underestimate the heat flux through each layer. The implication for the ocean is that it is likely to be thicker at times when the core is not convecting; in contrast, the crust will also lose heat more effectively when sub-critical, thus reducing its temperature and aiding crystallization (ocean thinning). However, the situation at the top of the ocean is more complex as crustal thickening increases the Rayleigh number to the power of three (Eq. (14)), thus accelerating the onset of convection and the validity of our assumed method of heat transfer. As we do not consider tidal heating, which is more than ten times lower than radiogenic

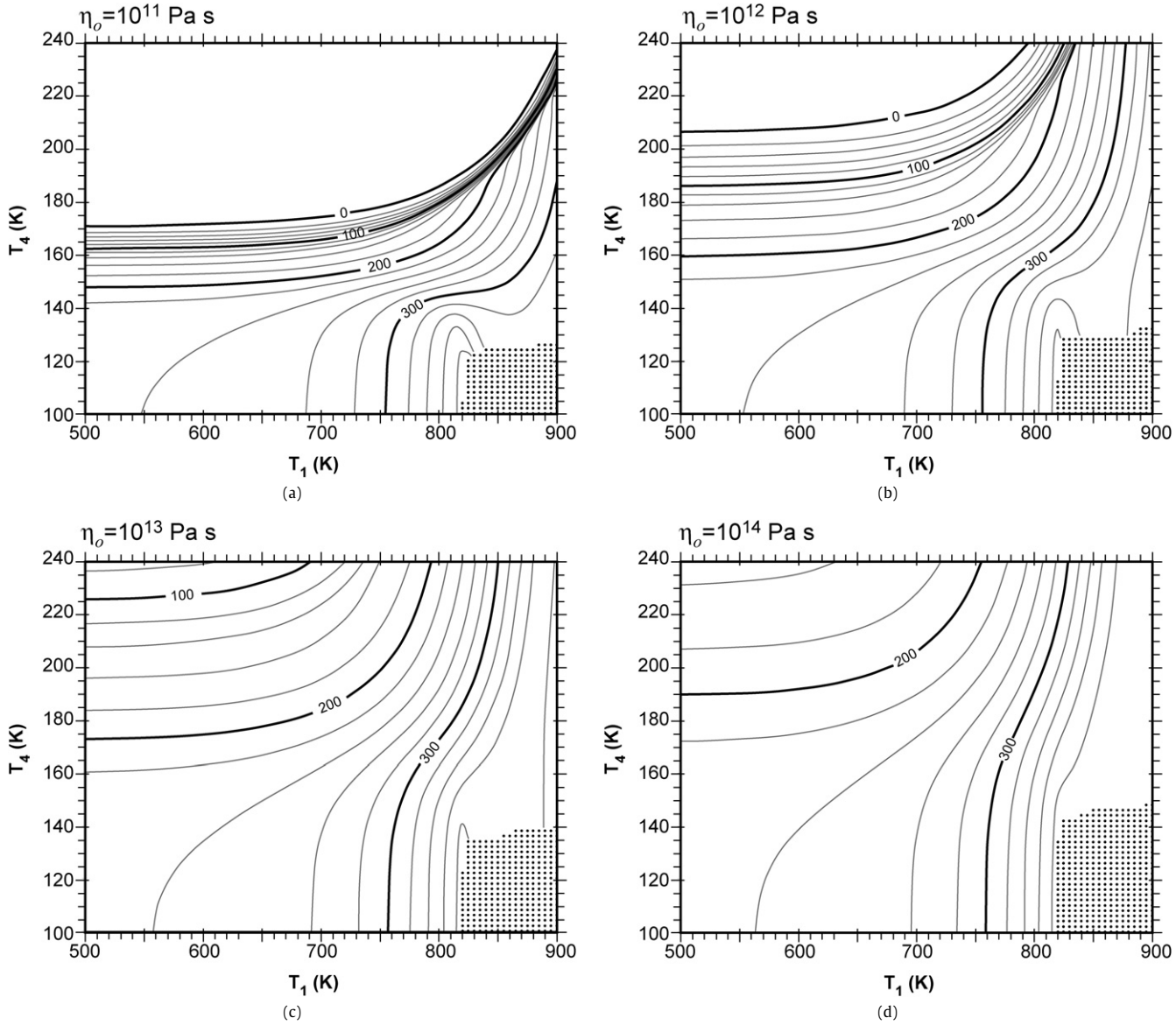

Fig. 12. Effect of initial temperatures and ice reference viscosity on the ocean thickness. In each case the thickness of the ocean is plotted in km as a function of initial core (T_1) and crustal (T_4) temperatures, for an ice reference viscosity of (a) 10^{11}; (b) 10^{12}; (c) 10^{13}; and (d) 10^{14} Pa s. Contour intervals are 20 km in each plot, and are generated from 5751 model runs in each case. Runs in which the ocean melted through are shown as filled circles, and were not used to generate the contours. All other parameter values are the same as in the nominal model.

heating for Titan (Sohl et al., 1995) but can still contribute some heat to our system, our estimates of ocean thickness are a minimum, and thus the likelihood of an ocean of aqueous ammonium sulfate persisting to the present day is feasible.

Our scaling laws assume a Newtonian rheology is applicable to the icy layers inside Titan. The rheology of ice under icy satellite conditions depends on a number of factors, including grain size, pressure, temperature, stress and ultimately, the deformation mechanism accommodating solid state creep (see Durham and Stern, 2001 for a review). Deformation in ice is accommodated by a combination of creep mechanisms, with the dominant mechanism dependent on the conditions (e.g., Goldsby and Kohlstedt, 2001). Diffusion creep, giving rise to a Newtonian rheology, is likely for ice which has a small grain size and is near its melting temperature (Barr and Pappalardo, 2005). There is no direct measurement of the grain size of ice on Titan, or the other icy moons for that matter. Terrestrial sea and polar ice have grain sizes typically of the order of 1–10 mm (Budd and Jacka, 1989; De La Chapelle et al., 1998); numerous studies of icy moons, Europa in particular, have argued for grain sizes which are typically of a similar, or smaller, range (e.g., Geissler et al., 1997; McKinnon, 1999; Nimmo and Manga, 2002; Nimmo, 2004). Small grain sizes which make diffusional flow more likely could be produced by the addition of other phases or contaminants, which pin the grain boundaries preventing growth (e.g., Kirk and Stevenson, 1987; McKinnon, 2006). Therefore we feel diffusion creep and Newtonian rheology are reasonable assumptions.

4.2. Implications for Titan's evolution

The process of ice I underplating a crust of mainly methane clathrate was discussed as a possible driving mechanism for cryovolcanism on Titan by Fortes et al. (2007). Our nominal model predicts about 50 km of underplated ice I after 4.5 Ga. However, rather than remain at the base of the crust, the low density ice I would create a Rayleigh–Taylor instability, whereby a small perturbation initiates diapiric rise of the ice through the denser overlying crust. We would expect this underplating and mixing process to

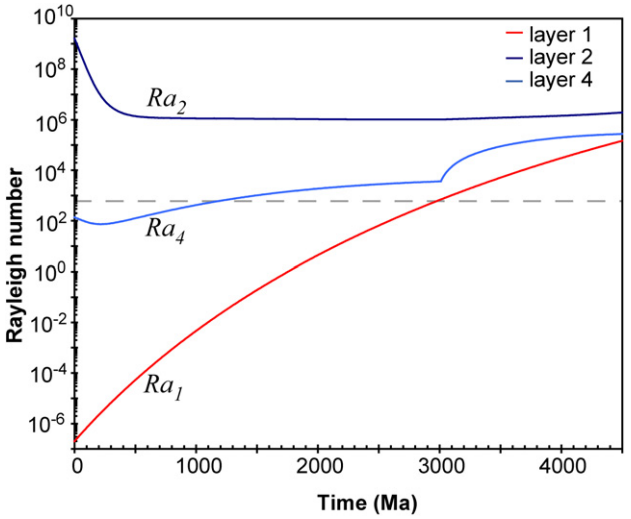

Fig. 13. Likelihood of convection in each layer. (a) Rayleigh numbers for the core (Ra_1), ice VI layer (Ra_2) and crust (Ra_4) for the nominal model. (b) Rayleigh numbers for the same layers and conditions, apart from a core starting temperature of 900 K, rather than 700 K. In both cases the dashed line shows a critical Rayleigh number for convection of 500.

be possible throughout the entire evolution, whenever ice I begins to add to the base of the crust (after ~3 Ga in the nominal model). The actual onset of diapiric rise in this situation requires a small perturbation to the interface layer, which then grows with time. The timescale of this growth depends on the wavelength and amplitude of the perturbation applied, and the density contrast between the two layers. We can estimate a likely growth timescale of the instability by using a simple linear stability analysis, which assumes that both the layers have the same viscosity (Turcotte and Schubert, 2002). For a 1 m initial perturbation of wavelength the same as the crustal thickness (123 km), then the diapir can penetrate to the surface in about 250 ka; for a perturbation wavelength of 50 km this timescale is increased to about 620 ka. The relatively quick times of diapir initiation and growth suggests that the underplated ice I will be incorporated continuously as it crystallizes. Stalled diapirs may occur in the crust where the ice I source region is depleted or if the density contrast is reduced (e.g., by contamination of the ice I diapir). These diapirs have been suggested as a potential mechanism for cryovolcanism on Titan (Fortes et al., 2007), and our thermal evolution model suggests that they will be common whenever the ocean has crystallized some ice I at its top boundary. For our nominal model this is after ~3 Ga, but varies depending on initial conditions and parameters chosen (Fig. 11). If the ocean increases in size over the evolution of Titan, then we would expect no ice I diapirs from underplating, and an alternative mechanism for cryovolcanism is required (e.g., topographic pumping—Showman et al., 2004; Fortes et al., 2007). The thinning of the crust in this case may actually increase the chance of fluids reaching the surface as a lower driving stress is required for upward percolation.

Approximately half of the models we consider would result in a dehydrated core, although this transformation is neglected in our models. In reality, the superheated water released during dehydration will lead to partial metasomatism of the core, and perhaps to melting, as occurs in the mantle wedge overlying dehydrating slabs on Earth (e.g., Bina and Navrotsky, 2000). This dehydration-related partial melting could then lead to volcanism at the rock–ice boundary; in our nominal model, dehydration would be expected after the core temperature has exceeded approximately 900 K at 2.8 Ga, although there is significant uncertainty in the exact location of the antigorite dehydration reaction, and therefore the exact timing of any subsequent core–mantle volcanism. However, such a region of partial melting makes an attractive habitat for astrobiological studies (e.g., Barr et al., 2001). The outermost layer (1–2 km) of the rocky core is probably sufficiently cool for organisms to survive; the maximum growth temperature for known terrestrial hyperthermophiles is 394 K. Any permeating liquid water can mediate a range of chemical reactions yielding substances of use to obligate anaerobes. The hydrostatic pressure at the base of the ice mantle is about 1.27–1.3 GPa, which is substantially greater than most organisms on Earth are adapted to. However, microbial metabolism has been reported at pressures of 1–1.2 GPa by Sharma et al. (2002); pressures greater than 1.6 GPa were found to kill the microbes under investigation. Although there is some dispute regarding the meaning of the formate oxidation observed in the latter experiments (e.g., Heremans, 2004), there is nothing to indicate that novel piezophilic organisms could not exist at such high pressures. We can speculate that the biochemistry, if based on carbon, will employ similar metabolic pathways to those found in deep terrestrial ecosystems (e.g., Pedersen, 2000). Alternatively, the biochemistry may be completely alien; Schulze-Makuch and Irwin (2006), for example, pointed out that low temperature serpentinization can lead to the formation of silanes, which might provide the basis for a polymerized silicon biochemistry quite unlike anything on Earth.

The release of methane from the breakdown of methane clathrate xenoliths in explosive cryovolcanic eruptions has been predicted for a cryomagma of aqueous ammonium sulfate (Fortes et al., 2007). Our parameter space survey suggests that one of the driving forces of this cryovolcanism, ice diapirs, begins for evolution times between about 3 and 0.5 Ga, and will continue until the present day. In the episodic model of Tobie et al. (2006), methane outgassing is predicted at three distinct time periods: (1) during core overturn, (2) at the onset of convection in the core, and (3) at the onset of convection in the crust. The Fortes et al. (2007) model predicts an initial methane outgassing episode during differentiation, followed by a more steady-state release over Titan's evolution as a result of cryovolcanism. Our model suggests that, neglecting driving mechanisms other than diapiric stress, cryovolcanism will most likely be important during the last 2–0.5 Ga of Titan's evolution. However, volcanism can also be expected even when diapiric rise is not; for example, the cold equivalent of a phreatomagmatic eruption would occur if a magma body encountered near-surface liquids, such as found in the north polar region (Stofan et al., 2007). We therefore believe it is more likely that volcanism, and associated methane outgassing, can occur throughout Titan's evolution, but with a marked increase in the last 0.5–1.5 Ga.

The final composition of the ammonium sulfate ocean, and of any surrounding crystallizates, can also be examined from the results of our model. In all model runs, the temperature of the ocean remains above the likely high pressure eutectic in the binary $(NH_4)_2SO_4$–H_2O system (Fortes et al., 2007). Thus we expect ice to be the only crystallization product of this system, although the composition of the ocean will become richer in ammonium sulfate as crystallization continues. This changing ocean composition will increase both the density and viscosity of the fluid, and will be important considerations for future studies of ocean dynamics on Titan.

5. Summary and conclusions

We have investigated the thermal evolution of a subsurface ocean of aqueous ammonium sulfate inside Titan. Crystallization of the ocean is controlled by the heat flux across it and the melting temperatures of the ice VI below, and crust (methane clathrate plus ice I) above. Cooling of the ocean leads to crystallization at both its top and bottom boundaries, and therefore thickening of the crust by ice I underplating, and of the ice VI layer from above. Underplating of the crust by ice I can lead to the formation of compositional buoyant diapirs, which have relatively short rise times compared to the evolution of Titan. For a wide range of initial parameters, the ocean does not crystallize completely over 4.5 Ga, and can therefore survive to the present day. Our nominal model predicts a heterogeneous crust that is 176 km thick, overlying an ocean 56 km thick.

Acknowledgments

P.M.G. is funded by the Science and Technologies Facilities Council (STFC) (Grant PP/C501992/1), and A.D.F. and L.V. by fellowships with the STFC (Grant PP/E006515/1) and The Royal Society respectively. We thank Steve Vance for a thorough review.

References

Andersson, O., Suga, H., 1994. Thermal conductivity of the Ih and XI phases of ice. Phys. Rev. 50, 6583–6588.

Barr, A.C., Pappalardo, R.T., 2005. Onset of convection in the icy Galilean satellites: Influence of rheology. J. Geophys. Res. 110, doi:10.1029/2004JE002371. E12005.

Barr, A.C., Pappalardo, R.T., Stevenson, D.J., 2001. Rise of deep melt into Ganymede's ocean and implications for astrobiology. Lunar Planet. Sci. XXXII. Abstract 1781.

Barr, A.C., Pappalardo, R.T., Zhong, S., 2004. Convective instability in ice I with non-Newtonian rheology: Application to the icy Galilean satellites. J. Geophys. Res. 109, doi:10.1029/2004JE002296. E12008.

Berman, R.G., Brown, T.H., 1985. Heat capacity of minerals in the system Na_2O–K_2O–CaO–MgO–FeO–Fe_2O_3–Al_2O_3–SiO_2–TiO_2–H_2O–CO_2: Representation, estimation, and high temperature extrapolation. Contrib. Mineral. Petrol. 89, 168–183.

Bina, C.R., Navrotsky, A., 2000. Possible presence of high-pressure ice in cold subducting slabs. Nature 408, 844–847.

Bridgman, P.W., 1937. The phase diagram of water to 45,000 kg/cm^2. J. Chem. Phys. 5, 964–966.

Budd, W.F., Jacka, T.H., 1989. A review of ice rheology for ice-sheet modeling. Cold Reg. Sci. Technol. 16, 107–144.

Castillo-Rogez, J., 2006. Internal structure of Rhea. J. Geophys. Res. 111, doi:10.1029/2004JE002379. E11005.

De La Chapelle, S., Castelnau, O., Lipenkov, V., Duval, P., 1998. Dynamic recrystallization and texture development in ice as revealed by the study of deep ice cores in Antarctica and Greenland. J. Geophys. Res. 103, 5091–5105.

Durham, W.B., Stern, L.A., 2001. Rheological properties of water ice—Applications to satellites of the outer planets. Annu. Rev. Earth Planet. Sci. 29, 295–330.

Durham, W.B., Kirby, S.H., Stern, L.A., Zhang, W., 2003. The strength and rheology of methane clathrate hydrate. J. Geophys. Res. 108, doi:10.1029/2002JB001872. 2182.

Ellsworth, K., Schubert, G., 1983. Saturn's icy satellites: Thermal and structural models. Icarus 54, 490–510.

Fortes, A.D., 2000. Exobiological implications of a possible ammonia–water ocean inside Titan. Icarus 146, 444–452.

Fortes, A.D., Grindrod, P.M., Trickett, S.K., Vočadlo, L., 2007. Ammonium sulfate on Titan: Possible origin and role in cryovolcanism. Icarus 188, 139–153.

Freeman, J., 2006. Non-Newtonian stagnant lid convection and the thermal evolution of Ganymede and Callisto. Planet. Space Sci. 54, 2–14.

Geissler, P.E., Phillips, C., Denk, T., 1997. The color of Europa: Comparisons with Ganymede, Callisto and Antarctica (No. 8.5). In: Workshop on Remote Sensing of Planetary Ices: Earth and Other Solid Bodies, Flagstaff, Arizona, June 11–13, 1996.

Giauque, W.F., Stout, J.W., 1936. The entropy of water and the third law of thermodynamics. The heat capacity of ice from 15 to 273°K. J. Am. Chem. Soc. 58, 1144–1150.

Goldsby, D.L., Kohlstedt, D.L., 2001. Superplastic deformation of ice: Experimental observations. J. Geophys. Res. 106, 11017–11030.

Grasset, O., Sotin, C., 1996. The cooling rate of a liquid shell in Titan's interior. Icarus 123, 101–112.

Grasset, O., Pargamin, J., 2005. The ammonia–water system at high pressures: Implications for the methane of Titan. Planet. Space Sci. 53, 371–384.

Grasset, O., Sotin, C., Dechamps, F., 2000. On the internal structure and dynamics of Titan. Planet. Space Sci. 48, 617–636.

Handa, Y.P., 1986. Compositions, enthalpies of dissociation, and heat capacities in the range 85 to 270 K for clathrate hydrates of methane, ethane, and propane, and enthalpy of dissociation of isobutane hydrate, as determined by a heat-flow calorimeter. J. Chem. Thermodyn. 18, 915–921.

Hauck, S.A., Phillips, R.J., 2002. Thermal and crustal evolution of Mars. J. Geophys. Res. 107, doi:10.1029/2001JE001801. 5052.

Heremans, K., 2004. Biology under extreme conditions. High Press. Res. 24, 57–66.

Howard, L.N., 1964. Convection at high Rayleigh numbers. In: Gortler, H. (Ed.), Proc. 11th Int. Conf. on Applied Mechanics. Springer-Verlag, New York, pp. 1109–1115.

Kirk, R.L., Stevenson, D.J., 1987. Thermal evolution of a differentiated Ganymede and implications for surface features. Icarus 69, 91–134.

Kivelson, M.G., Khurana, K.K., Volwerk, M., 2002. The permanent and inductive magnetic moments of Ganymede. Icarus 157, 507–522.

Klinger, J., 1973. Thermal conductivity of ice single crystals at low temperatures. In: Whalley, E., Jones, S.J., Gold, L.W. (Eds.), Physics and Chemistry of Ice. Royal Society of Canada, Ottawa, pp. 114–116.

Krivchikov, A.I., Gorodilov, B.Ya., Korolyuk, O.A., Manzhelii, V.G., Conrad, H., Press, W., 2005. Thermal conductivity of methane-hydrate. J. Low Temp. Phys. 139, doi:10.1007/s10909-005-5481-z.

Lodders, K., Fegley, B., 1998. The Planetary Scientist's Companion. Oxford Univ. Press, Oxford.

Lunine, J.I., Stevenson, D.J., 1987. Clathrate and ammonia hydrates at high pressure—Application to the origin of methane on Titan. Icarus 70, 61–77.

McKinnon, W.B., 1999. Convective instability in Europa's floating ice shell. Geophys. Res. Lett. 26, 951–954.

McKinnon, W.B., 2006. On convection in ice I shells of outer Solar System bodies, with detailed application to Callisto. Icarus 183, 435–450.

McNamara, A.K., van Keken, P.E., 2000. Cooling of the Earth: A parameterized convection study of whole versus layered models. Geochem. Geophys. Geosyst. 1. 2000GC000045.

Mishima, O., Môri, N., Endo, S., 1978. Thermal expansion anomaly of ice VI related to the order–disorder transition. J. Chem. Phys. 70, 2037–2038.

Moresi, L.N., Solomatov, V.S., 1995. Numerical investigation of 2D convection with extremely large viscosity variations. Phys. Fluids 7, 2154–2162.

Nimmo, F., 2004. Non-Newtonian topographic relaxation on Europa. Icarus 168, 205–208.

Nimmo, F., Manga, M., 2002. Causes, characteristics and consequences of convective diapirism on Europa. Geophys. Res. Lett. 29, 2109.

Nimmo, F., McKenzie, D., 1997. Convective thermal evolution of the upper mantles of Earth and Venus. Geophys. Res. Lett. 24, 1539–1542.

Nimmo, F., Stevenson, D.J., 2000. Influence of early plate tectonics on the thermal evolution and magnetic field of Mars. J. Geophys. Res. 105, 11969–11979.

Nimmo, F., Price, G.D., Brodholt, J., Gubbins, D., 2004. The influence of potassium on core and geodynamo evolution. Geophys. J. Int. 156, 363–376.

Pawley, A.R., Clark, S.M., Chinnery, N.J., 2002. Equation of state measurements of chlorite, pyrophyllite, and talc. Am. Mineral. 87, 1172–1182.

Pedersen, K., 2000. Exploration of deep intraterrestrial microbial life: Current perspective. FEMS Microbiol. Lett. 185, 9–16.

Phillips, R.J., Malin, M.C., 1983. The interior of Venus and tectonic implications. In: Hunten, D.M., Colin, L., Donahue, T.M. (Eds.), Venus. Univ. of Arizona Press, Tucson, pp. 159–214.

Prialnik, D., Bar-Nun, A., 1990. Heating and melting of small icy satellites by the decay of ^{26}Al. Astrophys. J. 355, 281–286.

Robie, R.A., Hemingway, B.S., 1995. Thermodynamic properties of minerals and related substances at 298.15 K and 1 bar (10^5 Pa) pressure and higher temperature. USGS Bull. No. 2131. US Government Printing Office, Washington, DC.

Ross, R.G., Kargel, J.S., 1998. Thermal conductivity of Solar System ices, with special reference to martian polar caps. In: Scmitt, B., de Beurgh, C., Festou, M. (Eds.), Solar System Ices. Kluwer, Dordrecht, pp. 33–62.

Ross, R.G., Anderson, P., Bäckstrom, G., 1977. Thermal conductivity of nine solid phases of H_2O. High Temp. High Press. 9, 87–96.

Ross, R.G., Anderson, P., Bäckstrom, G., 1978. Effects of H and D order on the thermal conductivity of ice phases. J. Chem. Phys. 68, 3967–3972.

Röttger, K., Endriss, A., Ihringer, J., Doyle, S., Kuhs, W.F., 1994. Lattice constants and thermal expansion of H_2O and D_2O ice I*h* between 10 and 265 K. Acta Crystallogr. B 50, 644–648.

Schubert, G., Ross, M.N., Stevenson, D.J., Spohn, T., 1988. Mercury's thermal history and the generation of its magnetic field. In: Vilas, F., Chapman, C.R., Mathews, M.S. (Eds.), Mercury. Univ. of Arizona Press, Tucson, pp. 429–460.

Schulze-Makuch, D., Irwin, L.N., 2006. The prospect of alien life in exotic forms on other worlds. Naturwissenschaften 93, 155–172.

Seipold, U., Schilling, F.R., 2003. Heat transport in serpentinites. Tectonophysics 370, 147–162.

Sharma, A., Scott, J.H., Cody, G.D., Fogel, M.L., Hazen, R.M., Hemley, R.J., Huntress, W.T., 2002. Microbial activity at gigapascal pressures. Science 295, 1514–1516.

Showman, A.P., Stevenson, D.J., Malhotra, R., 1997. Coupled orbital and thermal evolution of Ganymede. Icarus 129, 367–383.

Showman, A.P., Mosqueira, I., Head, J.W., 2004. On the resurfacing of Ganymede by liquid–water volcanism. Icarus 172, 625–640.

Shpakov, V.P., Tse, J.S., Tulk, C.A., Kvamme, B., Belosludov, V.R., 1998. Elastic moduli calculation and instability in structure I methane clathrate hydrate. Chem. Phys. Lett. 282, 107–114.

Slack, G.A., 1980. Thermal conductivity of ice. Phys. Rev. 22, 3065–3071.

Sohl, F., Sears, W.D., Lorenz, R.D., 1995. Tidal dissipation on Titan. Icarus 115, 278–294.

Sohl, F., Hussmann, H., Scwentker, B., Spohn, T., Lorenz, R.D., 2003. Interior structure models and tidal Love numbers of Titan. J. Geophys. Res. 108, doi:10.1029/2003JE002044.

Solomatov, V.S., 1993. Parameterization of temperature- and stress-dependent viscosity convection and the thermal evolution of Venus. In: Stone, D.B., Runcorn, S.K. (Eds.), Flow and Creep in the Solar System: Observations, Modeling and Theory. Kluwer, Dordrecht, pp. 131–145.

Solomatov, V.S., 1995. Scaling of temperature- and stress-dependent viscosity convection. Phys. Fluids 7, 266–274.

Solomatov, V.S., Barr, A.C., 2006. Onset of convection in fluids with strongly temperature-dependent, power-law rheology. Phys. Earth Planet. Int. 155, 140–154.

Solomatov, V.S., Moresi, L.-N., 2000. Scaling of time-dependent stagnant lid convection: Application to small scale convection on Earth and other terrestrial planets. J. Geophys. Res. 105, 21795–21817.

Sotin, C., Tobie, G., 2004. Internal structure and dynamics of the large icy satellites. C. R. Phys. 5, 769–780.

Sotin, C., Grasset, O., Beauchesne, S., 1998. Thermodynamical properties of high pressure ices: Implications for the dynamics and internal structure of large icy satellites. In: Schmitt, B., De Bergh, M., Festou, C. (Eds.), Solar System Ices. Klewer, Dordrecht, pp. 79–96.

Stevenson, D., Spohn, J.T., Schubert, G., 1983. Magnetism and thermal evolution of the terrestrial planets. Icarus 54, 466–489.

Stofan, E.R., and 37 colleagues, 2007. The lakes of Titan. Nature 445, 61–64.

Tchijov, V., 2004. Heat capacity of high-pressure ice polymorphs. J. Phys. Chem. Solids 65, 851–854.

Tobie, G., Grasset, O., Lunine, J.I., Mocquet, A., Sotin, C., 2005. Titan's internal structure inferred from a coupled thermal–orbital model. Icarus 175, 496–502.

Tobie, G., Lunine, J.I., Sotin, C., 2006. Episodic outgassing as the origin of atmospheric methane on Titan. Nature 440, 61–64.

Turcotte, D.L., Schubert, G., 2002. Geodynamics. Cambridge Univ. Press, Cambridge, UK.

Zimmer, C., Khurana, K.K., Kivelson, M.G., 2000. Subsurface oceans on Europa and Callisto: Constraints from Galileo magnetometer observations. Icarus 147, 329–347.